IEEE Access
Multidisciplinary | Rapid Review | Open Access Journal

Received April 27, 2018, accepted May 23, 2018, date of publication May 30, 2018, date of current version June 29, 2018.

*Digital Object Identifier 10.1109/ACCESS.2018.2842091*

# Image Skeleton and GA Based Tool Selection for 2 1/2-Axis Rough Milling

**JING WANG[1], MING LUO[1], (Member, IEEE), HAFIZ M. HAFEEZ[2], AND DINGHUA ZHANG[1]**

[1]Key Laboratory of Contemporary Design and Integrated Manufacturing Technology, Ministry of Education, Northwestern Polytechnical University, Xi'an 710072, China

[2]Beijing Jingdiao Group Co., Ltd., Beijing 102308, China

Corresponding author: Ming Luo (luoming@nwpu.edu.cn)

This work was supported by the China Major National Science and Technology project under Grant 2015ZX04001203.

**ABSTRACT** In the milling process, large tool diameter can get higher rigid and machining efficiency. To improve machining efficiency for 2 1/2-axis part, an image skeleton-based method is proposed in this paper. First, a rasterization-based method for converting the part section graphics into an image for image analysis with high accuracy is developed. Second, the Euclidean distance field is calculated for the image to get the initial skeleton; then to get the accurate skeleton of the image, a partial differential equation-based method is employed to refine the initial skeleton. After that, an objective function based on the residual area of the material is established, which is solved by the genetic algorithm to obtain the optimal tool combination for a given number of tools. Finally, the developed approach is validated in the milling of a port part for tool selection. Results show that the selected toolset can remove most of the material effectively. Furthermore, analysis results show that the increase of tool types will increase the available cutting area ratio, but it will decrease the growth.

**INDEX TERMS** Cutting tool, genetic algorithm, image analysis, milling, skeleton.

## I. INTRODUCTION

Complicated geometries such as pockets, sides and islands are often adopted in engine ports, mold and so on. Significant machining cost and machining time saving can be achieved by selecting a proper sequence of cutting tools [1]. However, determining the sequence of cutting tools is currently carried out by the trial and error testing, which is time-consuming and largely depends on engineer's experience [2], [3].

The selection of cutting tools for 2 1/2 -axis milling has been addressed by lots of researchers. Yao *et al*. [4] presented a geometric algorithm to determine the largest available cutting tool for 2D milling operation using a single cutter. Veeramani and Gau [5] proposed a two-phase methodology approach to determining an optimal set of cutting tool size for 2.5D pocket machining. Lim *et al*. [6] discussed an algorithm for calculating the volume of a 2D-profile, accessible by a given diameter of the milling cutter. Later, they presented a method for determining a theoretically optimal combination of cutting tools given a set of 3D volumes or 2D profiles [7]. Optimal tools are selected by considering residual material that is inaccessible to oversized cutters and the relative clearance rates of cutters that can access these regions of the selected machining features. Lee and Chang [8] discuss a methodology of applying computational geometry techniques to extract machining information of geometric constraints from a given complex surface design to support the process planning. Chen and Zhang [9] proposed an approach to determine the largest allowable size for the cutter to move along all the profiles in 2 1/2 -axis finish machining without global and local gouging. Later they proposed an optimal approach for multiple tool selection and their numerical control path generation for aggressive roughing of the pocket by using the pocket's medial axis transform [10]. Kim and Woo [11] proposed a method to detect virtual corners and to calculate the maximum cutter sizes with the virtual corner detection for planar milling. Mejia-Ugalde *et al*. [12] presented a new method based on directional morphological approaches, applied to automatic tool selection in computer numerical control milling machines for machining a 2.5D of a geometry piece provided of a three-dimensional model of computer-aided design or from an image taken with other devices. Chen and Liu [13] proposed an intelligent approach for multiple standard cutters of maximum sizes for three-axis sculpture surface machining and hybrid global optimization method is used. Ahmad *et al*. [14] presented a systematic



2169-3536 © 2018 IEEE. Translations and content mining are permitted for academic research only.
Personal use is also permitted, but republication/redistribution requires IEEE permission.
See http://www.ieee.org/publications_standards/publications/rights/index.html for more information.

method to select the optimal sequence of tool(s), to machine a 2.5-axis pocket given the pocket geometry, a database of cutting tools, cutting parameters, and tool holder geometry. A Genetic Algorithm (GA) formulation is then used to find the optimal tool sequence. In all, these existing methods mainly use the geometrical information for cutter size calculation. However, this method also has the following limitations: (1) Calculation process is complex. Separation of the original shape and calculation iteration are needed. (2) It is mainly used for closed area. For open area or area with holes, it is difficult to calculate. (3) For an area with multi branches, it is prone to get wrong results.

The skeleton can provide the size and shape information of an image target, and thus has an important position in digital image analysis [15], [16]. The image skeleton can be used for shape matching and retrieval for searching and comparing 3D objects [17] or scatterplot diagnostics to automatically find potentially interesting plots [18]. However, little research has been done to apply image skeleton in the machining process for tool selection or path planning.

To this end, this paper proposes a new image skeleton based tool diameter selection method for 2 1/2 -axis milling. Since a 2D image can be used for describing any complex profile, it is employed the first time to represent the 2D workpiece in this study. Firstly, graphics rasterization method is developed to get a high-resolution image of parts and the skeleton is then extracted from the image. After that, an intelligent tool selection method with GA is developed based on the image skeleton to calculate the suitable cutting tool sizes. Finally, the developed method is validated by selecting cutting tools for milling of a port part. The contribution of this paper is that an image skeleton based tool diameter selection method is presented, and it can be used for a part with complex boundaries, including open loop and holes.

## II. METHODOLOGY

While planning toolpath for 2 1/2 -axis rough milling, the tool diameter should be large enough to improve the machining efficiency. A suitable tool should be the one tangent with boundaries around it. The application of image skeleton to solve manufacturing problems is a new approach in the field of tool selection for machining. In this article, approaches to getting the automatic tool sequence using image skeleton are proposed. In this way, the original part is a 3D model taken from CAD software and its section graphics are extracted; then by applying a transformation into image files. In order to get high revolution part section image, graphics rasterization operation is applied. After that, the image skeleton is extracted for every part section image and then tool radius variation along the skeleton are calculated. Finally, the objective function for tool selection is established to get minimum uncut material and the optimization problem is solved by applying Genetic Algorithms (GA). Fig. 1 shows the overall steps for intelligent tool selection based on the image skeleton, and each step is discussed in the following sections.

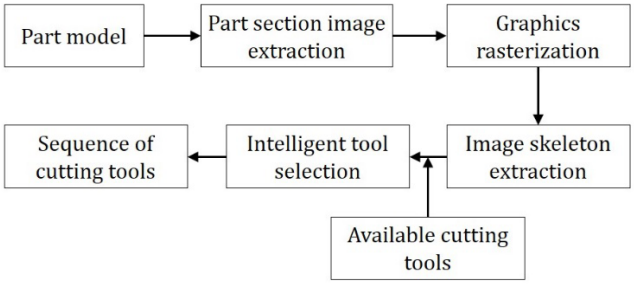


**FIGURE 1.** Overall methodology.

## III. GRAPHICS RASTERIZATION

The calculation of skeleton of an image is already well developed and is quick and stable, it will be applied to a binary image in this study. However, the main disadvantage of this method is that its calculation accuracy is based on the image pixel precision. In this article, section graphics of a part is transferred to binary images, as shown in Fig. 2. Therefore, to get accurate tool selection results, it is necessary to get high pixel accuracy. In order to achieve the above objective, a graphics rasterization technology is developed here.

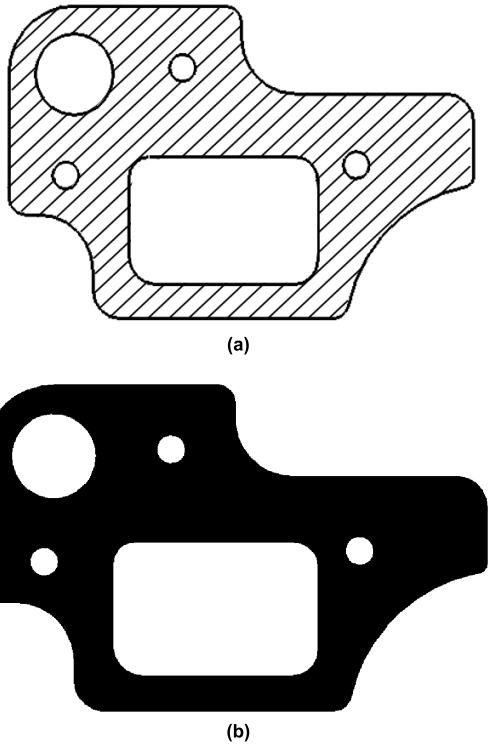


**FIGURE 2.** Part section graphics and transformed image. (a) Section graphics. (b) Transformed image.

Loss of accuracy is valid when transforming a graphics to an image, it mainly comes from two aspects: (1) Approximation of original shape with a polygon. During the transformation from graphics to image, shape contour is extracted first and used to determine the image boundary. Polygon approximation is usually used in this procedure and error

is introduced. (2) The increase of distance can only be measured with the pixel in an image, it's not continuous. Therefore, the image skeleton and the medial axis of corresponding graphics are not completely coincided. In order to get the accurate image skeleton for the tool selection, transformation accuracy must be controlled. Tool selection will not be affected when the transformation accuracy is well controlled.

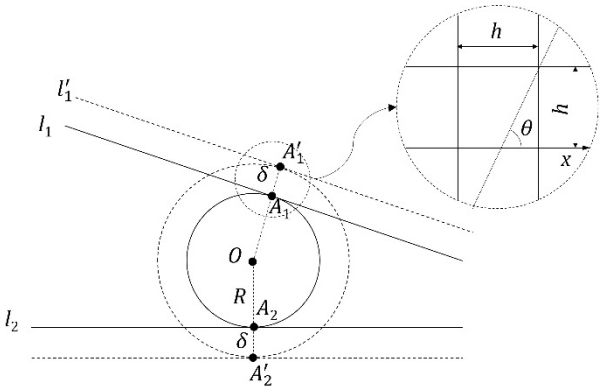


**FIGURE 3.** From graphics to image.

Firstly, the influence of the distance discontinuous is analyzed. While machining of a shape contour, the machining accuracy is mainly affected by the tool diameter. Therefore, the transformation accuracy can be determined by the tool diameter. As shown in Fig. 3, let the minimum increment of the tool diameter be $2\delta$, the pixel width is $h$. When the angle $\theta$ between $OA_1$ and $x$ axis locates between 0° and 45°, pixel increments can be controlled within one pixel if the distance in the image is less than $\frac{h}{\cos\theta}$; when the angle locates between 45° and 90°, pixel increments can be controlled within one pixel if the distance in the image is less than $\frac{h}{\sin\theta}$. Therefore, in order to control the transformation accuracy, distance in the image should be less than $min\left\{min\left\{\frac{h}{\cos\theta_1}\right\}, min\left\{\frac{h}{\cos\theta_2}\right\}\right\}$ when the tool diameter increment is $\delta$, where $\theta_1 \in [0°, 45°]$, $\theta_2 \in (45°, 90°]$. That is to control the distance less than the pixel width $h$.

If tiny perturbation $\varepsilon$ occurs during the transformation from the graphics to an image, increase or decrease of one pixel is possible and it will lead to tool radius increase $\delta$. Tool radius is too sensitive to tiny perturbation $\varepsilon$. In order to solve this problem, double enlarge of the image is applied in this study. That is, when tool radius increase $\delta$, the corresponding distance in the images is $2h$. Then the actual size of every pixel is $\lambda = \frac{\delta}{2h}$. Usually, the minimum increase of tool diameter is 1mm and $\delta = 0.5mm$. The width of every pixel is $h = 1$, therefore the actual width $\lambda$ of every pixel is $\lambda = 0.25mm$. By applying the proposed method, the transformation accuracy can be controlled for the tool selection process.

Secondly, the approximation accuracy of the original shape contour with the polygon is analyzed below. In order to get high approximation accuracy, the chord height tolerance controlling is used in this article. As shown in Fig. 4, in order

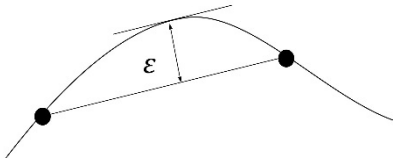


**FIGURE 4.** Discrete error control.

to guarantee the original graphics is close to the transformed image, the chord height should be controlled as $\varepsilon < \frac{\lambda}{2}$. As analyzed above, $\lambda = \frac{\delta}{2h}$, therefore chord height should be $\varepsilon < \frac{\lambda}{4h}$.

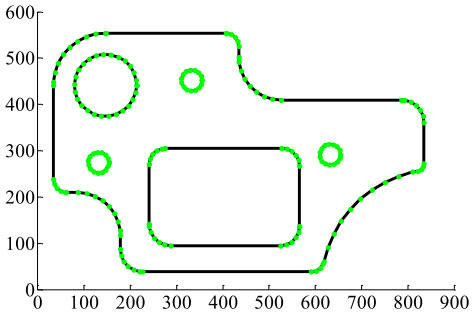


**FIGURE 5.** Approximation polygon.

Shown in Fig. 5 is the example of an approximated polygon, green points represent the discrete points under the chord height $\varepsilon$. When the approximation polygon is obtained, the scan-line fill algorithm is applied in this article to fill the approximated polygon, and Fig. 6 shows the filled result.

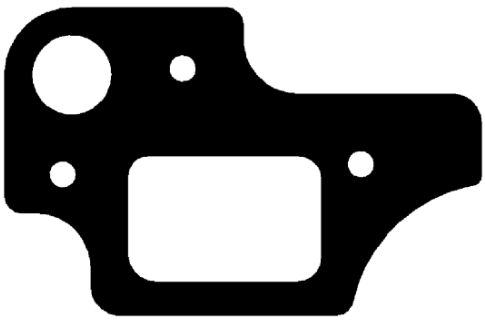

**FIGURE 6.** Image after rasterization.

## IV. EXACT IMAGE SKELETON EXTRACTION

The calculation of image skeleton is the basis for the tool selection. In this section, the Euclidean distance field is calculated first to get an initial skeleton. After that, the initial image skeleton is transformed to get an accurate skeleton. Finally, the maximum feasible tool diameter for every point is determined based on the image skeleton.

### A. EUCLIDEAN DISTANCE FIELD

The calculation of distance field is one of the basic technology in computer graphics, it is actually an image

transformation method and widely used in image processing. For two points $\boldsymbol{A}(x_A, y_A)$ and $\boldsymbol{B}(x_B, y_B)$ in a given image, the Euclidean distance is $d(\boldsymbol{A}, \boldsymbol{B}) = \sqrt{(x_B - x_A)^2 + (y_B - y_A)^2}$, and $x$ and $y$ refer to the row number and column number. The distance field of a binary image can be defined as the set of the minimum distance between the set of pixels and image sets of boundary pixels. The minimum distance between each pixel and set of boundary pixel is needed, but the computing process is time-consuming. To save computation time, the ordered Propagation method is applied.

### B. IMAGE SKELETON EXTRACTION

There are four methods to extract the skeleton of a binary image: (1) Mathematical morphology [19]. It can be used for fast image skeleton extraction, but the result is not accurate enough for the binary image. (2) Distance Transform [20]. The method can get an accurate image skeleton but the connexity cannot be guaranteed. (3) Voronoi diagram [21]. It is based on the sampling points and the complexity increased rapidly with the increase of accuracy requirement. (4) Partial differential equations based method [22]. This method usually combines the distance field and moves to the skeleton position through the initial curve under the action of the external force and the internal force of the distance field. Therefore, it has high calculation accuracy and a good anti-noise performance. In this research, the dynamic skeleton method, which is one of the partial differential equations based method, is employed for skeleton extraction.

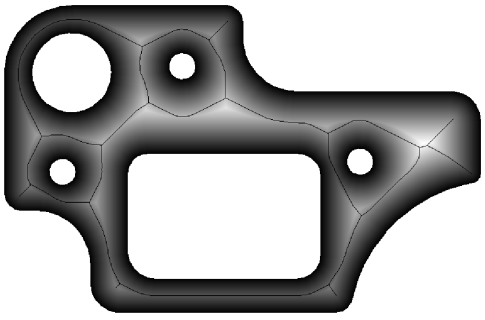

**FIGURE 7.** Initial skeleton extracted with mathematical morphology.

The initial skeleton is extracted with the mathematical morphology method, as shown in Fig. 7. The blank curve is the extracted initial skeleton, it can be seen that it does not completely overlap with the white ridge curve of the distance field. Therefore, further refinement is needed to get the accurate skeleton.

In order to get the exact skeleton, the snake model proposed by Kass *et al.* [23] is employed here for localizing edges accurately. A snake is a controlled continuity spline under the influence of internal energy and external energy. The internal spline forces serve to impose a piecewise smoothness constraint. The external constraint forces are the response for putting the snake near the desired location. When the snake deforms, the minimum energy should be reached. That is, the total energy should be the minimum. The total energy function $E(\boldsymbol{r}(t))$ of the Snake model is

$$E(\boldsymbol{r}(t)) = \int_0^1 (E_{int}(\boldsymbol{r}(t)) + E_{ext}(\boldsymbol{r}(t))) \tag{1}$$

where $\boldsymbol{r}(t) = (x(t), y(t)), t \in [0, 1]$ is the parameter function of part contour, $(x(t), y(t))$ are the $x$ and $y$ coordinates on the contour, $E_{int}$ represents the internal energy of the contour, $E_{ext}$ is the external energy of the contour. The internal energy $E_{int}$ is used to control the contour continuity and smoothness, it is expressed as

$$E_{int}(r(t)) = \frac{1}{2}\left(\alpha \left|\frac{d\boldsymbol{r}(t)}{dt}\right|^2 + \beta \left|\frac{d^2\boldsymbol{r}(t)}{dt^2}\right|^2\right) \tag{2}$$

Within the above equation, the first item is used to suppress the curve length, the second item is used to maintain the smoothness of the curve, $\alpha$ and $\beta$ are used to control the flexibility and stiffness of $E_{int}$, their value affects the sensitivity of $E_{int}$ in the contour controlling process. The external energy $E_{ext}$ is used to control the contour to move towards the target boundary of image $I$, and it is expressed as

$$E_{ext}(\boldsymbol{r}(t)) = -|\nabla(G_\sigma(\boldsymbol{r}(t)) \cdot I(\boldsymbol{r}(t)))|^2 \tag{3}$$

where $G_\sigma(\boldsymbol{r}(t))$ is the Gauss function with a standard deviation of $\sigma$, and $I(\boldsymbol{r}(t))$ is the gray value of the contour in image $I$. Since $I$ is the Euclidean distance field, its value is the shortest distance to the image boundary from the corresponding point on the contour $\boldsymbol{r}(t)$.

While using the snake model, a single point cannot be reached since the potential is not equal for each point on the ridge line in most cases. Besides, it will be very complex to use only one snake for the skeleton refinement. In this paper, the initial skeleton is decomposed into segments for later refinement, and constraints exist for each decomposed segment. Therefore, refinement for each segment must be followed by sequence.

#### 1) SKELETON DECOMPOSITION

Each edge of the initial skeleton is assigned as a snake in the decomposition process, a closed loop is assigned as a closed snake. Define the non-closed edge as a single edge, and define points that not connected with other single edge or closed loop as leaf point. Define the depth $d_V$ of vertex $\boldsymbol{V}_a$ as:

$$d_V(\boldsymbol{V}_a) = \begin{cases} 1 & \text{if } \boldsymbol{V}_a \text{ is the leaf point or locates on the loop} \\ \min\limits_{\boldsymbol{V}_b \in (\boldsymbol{V}_a)} (d_v(\boldsymbol{V}_b)) + 1 & \text{if } N(\boldsymbol{V}_a) \text{ is the adjacent vertices of } \boldsymbol{V}_a \end{cases} \tag{4}$$

According to the depth $d_V$, the priority weight $(W)$ of the edge can be defined as:

$$W(\boldsymbol{r}) = \begin{cases} 0, & \boldsymbol{P} = \boldsymbol{Q} \\ \min(d_v(\boldsymbol{P}), d_v(\boldsymbol{Q})), & \boldsymbol{P} \neq \boldsymbol{Q} \end{cases} \tag{5}$$

where $\boldsymbol{P}$ and $\boldsymbol{Q}$ are two vertices on the snake spline $\boldsymbol{r}$.

#### 2) SKELETON REFINEMENT

The initial skeleton should be refined and the refinement should be done followed by sequence. After defining the weight, smaller weights will be refined first. For those that have the same weights, the order can be arbitrary. According to the above order, the final refined skeleton can be obtained. The objective function $E$ should be defined for the refinement process. For calculation simplicity, a cubic B-spline is used to represent the snake spline. It implies the smoothness constraint, the internal energy cannot be taken into consideration. Let $\{\boldsymbol{P}_i | i = 0, 1, \ldots, n\}$ be the control points, then the B-spline function $\boldsymbol{r}(t) = (x(t), y(t))$ can be expressed as:

$$\boldsymbol{r}(t) = \sum_{i=0}^{n} N_{i,k}(t) \boldsymbol{P}_i, \quad t \in [0, 1] \tag{6}$$

By submitting the above equation into the energy function $E(\boldsymbol{r}(t))$, the following can be derived

$$E(\boldsymbol{r}(t)) = -\sum_{i=0}^{n} \left( \left( \frac{\partial (G_\sigma (\boldsymbol{r}(t)) \cdot I(\boldsymbol{r}(t)))}{\partial x(t)} \right)^2 + \left( \frac{\partial (G_\sigma (\boldsymbol{r}(t)) \cdot I(\boldsymbol{r}(t)))}{\partial y(t)} \right)^2 \right) \tag{7}$$

According to the above refinement, each edge of the initial skeleton will fall on the ridge line of the distance field and the exact skeleton can be obtained. Based on the exact skeleton, tool radius distribution along the skeleton can be determined. Fig. 8 shows the exact skeleton of the image after refinement using the Snake energy function as well as the corresponding tool diameter distribution.

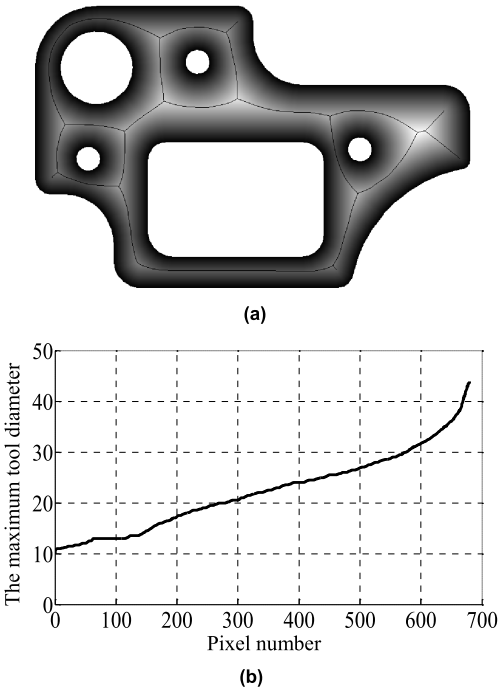


**FIGURE 8.** The exact skeleton of the image and the corresponding tool diameter distribution. (a) The skeleton after correction. (b) The tool diameter distribution.

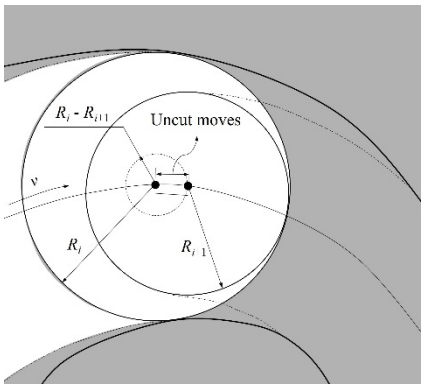


**FIGURE 9.** Adjustment of start point.

## V. GA BASED TOOL SELECTION

Tool radius distribution along the skeleton shows the largest tool that can be used for each point. However, in the practical machining process, only limited number of tools can be used. This section discusses how to select proper tools according to certain constraints.

### A. ANALYSIS OF THE MACHINING AREA

In most cases, a set of cutting tool will be used in order to improve machining efficiency. A larger cutter is used first to remove a large amount of raw material, and smaller cutters are used later to remove rest uncut raw material.

While calculating the residual uncut area for tool diameter selection, the total area for each tool that can be cut should be summed first. It is difficult for area calculation with irregular boundary graphics, however, it is easy after transforming into an image. Since the distance field and skeleton are already obtained, the distance between a point on the skeleton and the machined area boundary can be obtained. After calculating the tool diameter for each point on the skeleton curve, the value for every point within the tool profile will be changed, from 0 (uncut) to 1 (cut) for example. After that, all the remaining pixel with value 0 are uncut, the residual uncut area can be calculated. However, there still exits the following problems:

- In the milling process, tools with a larger diameter will be used first, then tools with a smaller diameter. While using smaller cutting tools, the starting point usually coincides with the end point of the larger cutting tool. It is easy to handle but uncut moves exist, as shown in Fig. 9. For this case, the start point can be moved along the skeleton to have the tool contacted with the uncut boundary to avoid air cut segment.
- When a cutting tool moves to the end of the skeleton branch, the uncut region may exist due to the actual cutting tool radius is smaller than the calculated one, as shown in Fig. 10. The end point is extended until the cutting tool reaches the image boundary.

### B. ESTABLISHMENT OF THE OBJECTIVE FUNCTION

Given the available set of cutting tools $\Omega = \{R_i | i = 1, 2, \ldots, n\}$, there are two methods to improve the

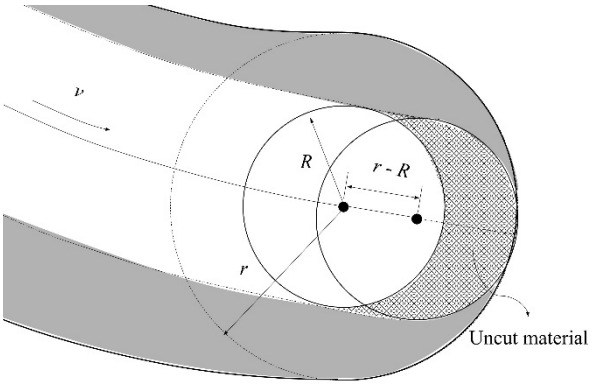


**FIGURE 10.** Extension of end point.

machining accuracy: (1) Number of cutting tools are constant, improve machining efficiency can be achieved by changing the cutting tool radius combination. (2) Improve machining efficiency is reached by increasing the cutting tool number. As for the second one, it will lead to the increase of preparation workload. Therefore, the objective function for intelligent tool selection is constructed according to the first method in this article. Given cutting tool number $m \leq n$, taken the rest uncut raw material as the objective function of tool set selection problem, it can be expressed as:

$$\begin{cases} \min f(x_1, \ldots, x_m) = s_m \\ s.t\ x_i \in \Omega \\ \quad x_i > x_{i+1} \end{cases} \tag{8}$$

where $S_m$ is the area of rest uncut material after machining along the image skeleton. The cutting tool is listed according to its radius in the cutting tool set.

### C. TOOL SELECTION

Due to high nonlinearity of the problem, the established model is a complex optimization problem. The GA is often used to solve the optimization problems. Genetic algorithms mainly include elements such as population initialization, fitness function building, and genetic manipulation.

#### 1) POPULATION INITIALIZATION

Since the radius increment is discontinuous, it is difficult to encode the cutting tool radius directly. In this article, the cutting tool in set $\Omega$ is numbered from 0 to $n-1$. The number is encoded with 0/1 binary mode and the binary bits (a) satisfy $2^a - 1 \leq n \leq 2^{a+1} - 1$. Since multi-tool will be used in the machining process, it is necessary to put all cutting tool numbers in one population sequentially. The total available bits are $ma$, and $m$ is the total number of cutting tools. For example, the following code can be obtained when $a = 4$ and $m = 5$, and the code represents that the tool set includes five different tools: 1, 3, 4, 9 and 12.

$$\underbrace{0001}_{1}\,\underbrace{0011}_{3}\,\underbrace{0100}_{4}\,\underbrace{1001}_{9}\,\underbrace{1100}_{12}$$

A population is a collection of individuals. After the coding of individual parameters, these encoded individuals should be grouped into the corresponding population. Assuming that the initial population size is H, then initialize solutions of such population randomly, and the initial solution for each population is a randomly generated $ma$-bit 0/1 code.

#### 2) ESTABLISHMENT OF THE FITNESS FUNCTION

The fitness function is mainly used to distinguish individuals in a population from each other and is an indicator for evaluating the merits of individuals. For binary coding in the above-mentioned populations, it is necessary to convert to real number coding and perform fitness function calculation. Since the objective is to find the minimum value of function $f(x)$, the following fitness function can be established:

$$F(f(x)) = \frac{1}{f(x)} \tag{9}$$

In the above equation, the smaller the individual function $f(x)$, the greater the fitness value and the better the individual. To calculate the minimum value of $f(x)$, let

$$\begin{aligned} s_i &= \min(\mathcal{A}_1, \cdots, \mathcal{A}_H) \\ S_m &= \min(s_1, \cdots, s_L) \end{aligned} \tag{10}$$

where $H$ is the population size, $L$ is the maximum generation, $s_i$ is the minimum area of uncut material of $i^{th}$ generation, $\mathcal{A}_k$ is the uncut material area by using cutting tool of $k_{th}$ population of certain generation, $S_m$ is the minimum uncut material area of all generation. In this way, the minimum value of $f(x)$ is $S_m$.

#### 3) GENETIC MANIPULATION

The genetic manipulation mainly includes selection, crossover, and mutation, the purpose is to generate the new population from the current population in order to obtain better individuals. The purpose of the selection is to obtain fathers for crossover and mutation, the main methods include roulette, tournaments, etc. The Roulette method is used here as an individual selection method. The probability of each individual being selected is

$$p_i = \frac{F_i}{\sum F_i} \tag{11}$$

where $F_i$ is the fitness value for the $i$th individual.

As shown in Fig. 11, the crossover refers to the random selection of two individuals in a population. By swapping and combining the two chromosomes, the parent's excellent characteristics are passed on to the offspring, thereby creating new excellent individuals. The mutation refers to randomly selecting an individual in a population and mutating at a certain point in the individual to generate a new individual. Its purpose is to maintain the population diversity and prevent the optimization process from falling into a local optimum.

Numbers of chromosomes are needed to form a population, each chromosome contains a certain number of genes. Whether the gene can be obtained will be determined by

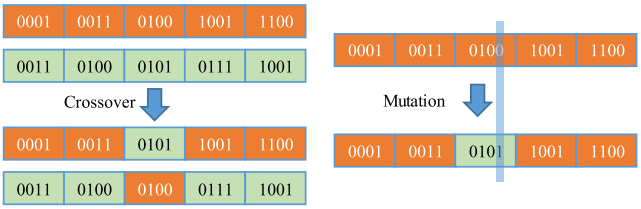


**FIGURE 11.** Crossover, and mutation in genetic manipulation.

0/1 code; the crossover and mutation of chromosomes will generate the next generation population of chromosomes. In this research, the population H is crossed or mutated to get a new generation of the population, and the final optimized results will get by several generations.

Take the number of generation L and carry out the initial population calculation for the first generation, get the tool group randomly according to the probability $p_i$ of each individual being selected. The crossover rate and mutation rate are then used to determine whether the crossover or mutation occurs.

If the crossover between two sets of cutting tool occurs, select any crossover position and change all binary codes after that position. Then the generated new codes have to be checked to determine whether the selected cutting tools are available or not.

If the mutation of a certain set of cutting tools occurs, select a mutation position randomly and encode it with 0/1 code. Then the generated new codes have to be checked to determine whether the selected cutting tools are available or not.

After calculation for all generation, an optimal set of the cutting tools can be selected by comparing selected cutting tool set of every generation and cutting tool sets of all generation.

The maximum generation L and population size H are determined by the problem scale, the cross rate is set to 0.7 and the mutation rate is set to 0.001 according to experience.

## VI. RESULTS AND DISCUSSION

Fig. 12(a) shows an example of a port part for 2.5D milling with different depths. The selected tool range is [10] and [43] and two cutting tools in the set will be selected. The proposed method is applied and the optimized results are Φ25 and Φ11.

Shown in Fig. 13 are the maximum available tool diameter along the image skeleton for section shown in Fig. 12(b). The available range for tool Φ11 is $[a_1, a_2]$ and the available range for Φ25 is $[a_2, a_3]$. To compare the machining efficiency between conventional method based on experience and the developed new approach, a flat end milling cutter with radius of 5.5mm is selected using the conventional way to machine the part. The machining time by using these two methods are listed in Table 1. It is apparent that the total machining time by using one end milling cutter is 8.28min, while that by using multiple optimum end milling cutters is 6.55min, which is about 80% of the machining time taken by the conventional method. Therefore, the proposed approach can increase the machining efficiency and reduce the manufacturing costs. The residual uncut area after two tools is shown in Fig. 14.

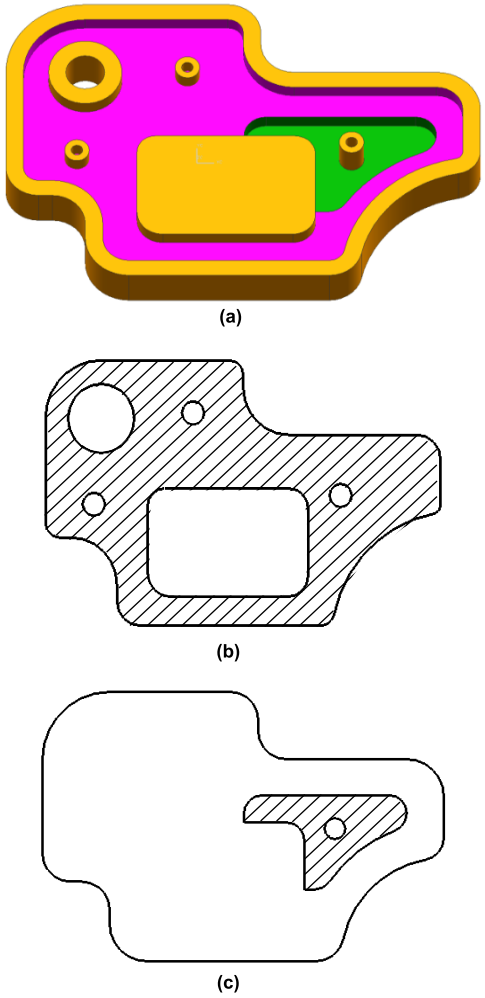


**FIGURE 12.** Part model and section view. (a) 3D part model. (b) Layer 1. (c) Layer 2.

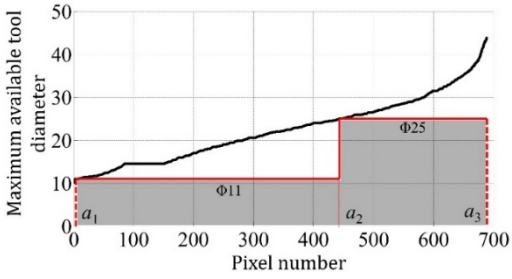


**FIGURE 13.** Tool diameter distribution.

**TABLE 1.** Machining time by using the conventional and the proposed approach.

| Machining type | New approach | | | Conventional method |
|---|---|---|---|---|
| | Radius (12.5mm) | Radius (5.5mm) | Total | Radius (5.5mm) |
| Machining time(min) | 2.22 | 4.33 | 6.55 | 8.28 |

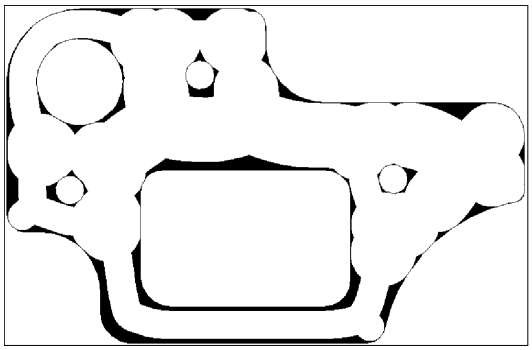

**FIGURE 14.** The residual uncut area after cutting with two tools (Φ 25 and Φ 11).

Furthermore, if the tool number is set to 5, which means five different diameters can be used, the optimized tool diameters are 33, 24, 19, 14 and 11, as shown in Fig 15. The cut area ratio for each tool is shown in Table 2, and the residual uncut area after five tools is shown in Fig. 16.

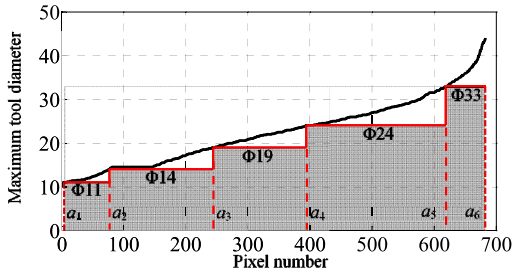


**FIGURE 15.** Tool diameter distribution with five tools.

**TABLE 2.** Machining area covered by 5 different tools.

| Tool diameter (mm) | Cut area ($mm^2$) | Area ratio (%) |
|---|---|---|
| 33 | 17441.50 | 33.10 |
| 24 | 20182.75 | 38.3 |
| 19 | 6080.50 | 11.54 |
| 14 | 4992.75 | 9.48 |
| 11 | 1968.50 | 3.74 |
| Total | 50666 | 96.16 |

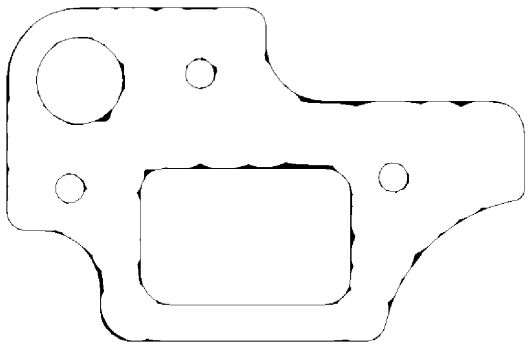

**FIGURE 16.** The residual uncut area after five tools.

While considering the second layer, the distance field and its skeleton is shown in Fig. 17(a), the corresponding tool diameter distribution is shown in Fig. 17(b).

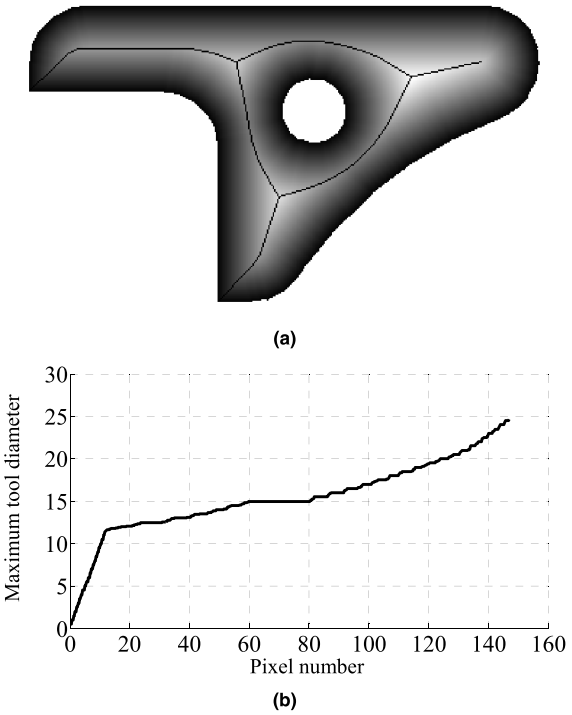


**FIGURE 17.** Extracted image skeleton and tool diameter distribution for the second layer. (a) Extracted image skeleton for the second layer. (b) Tool diameter distribution.

In the milling process, tool selection for both layers with different depth should be considered together, then the tool diameter distribution is shown in Fig. 18.

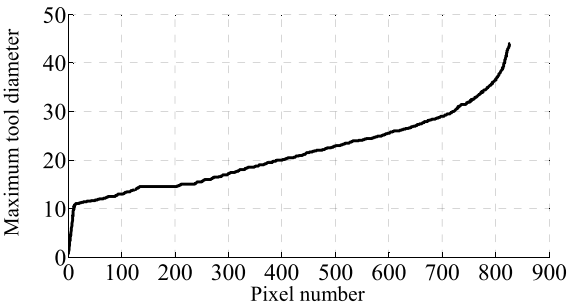


**FIGURE 18.** Tool diameter distribution for both layers.

**TABLE 3.** Machining with two tools.

| Tool diameter (mm) | Cut area ($mm^2$) | Area ratio (%) |
|---|---|---|
| 25 | 35940.97 | 58.35 |
| 12 | 16581.51 | 26.92 |
| Total | 52522.48 | 85.27 |

Suppose the available tool diameter set is $\Omega = \{1, 2, 3, 4, 5, 6, 8, 10, 12, 16, 20, 25, 28, 30, 35, 40\}$, if only two types of tool are allowed, then the optimization results are 25mm and 12mm. In this case, the total area ratio can be cut is 85.27%, Which is shown in Table 3. Too much material is

**TABLE 4. Machining with three tools.**

| Tool diameter (mm) | Cut area ($mm^2$) | Area ratio (%) |
|---|---|---|
| 28 | 29237.50 | 47.47 |
| 20 | 18813.50 | 30.54 |
| 12 | 7840.75 | 12.73 |
| Total | 55891.75 | 90.74 |

**TABLE 5. Machining with four tools.**

| Tool diameter (mm) | Cut area ($mm^2$) | Area ratio (%) |
|---|---|---|
| 28 | 29237.50 | 47.47 |
| 20 | 18813.50 | 30.54 |
| 12 | 7840.75 | 12.73 |
| 8 | 1041.50 | 1.69 |
| Total | 56933.25 | 92.43 |

**TABLE 6. Machining with five tools.**

| Tool diameter (mm) | Cut area ($mm^2$) | Area ratio (%) |
|---|---|---|
| 28 | 29237.50 | 47.47 |
| 20 | 18813.50 | 30.54 |
| 16 | 3109.00 | 5.05 |
| 12 | 5359.50 | 8.70 |
| 10 | 1304.75 | 2.12 |
| Total | 57824.25 | 93.88 |

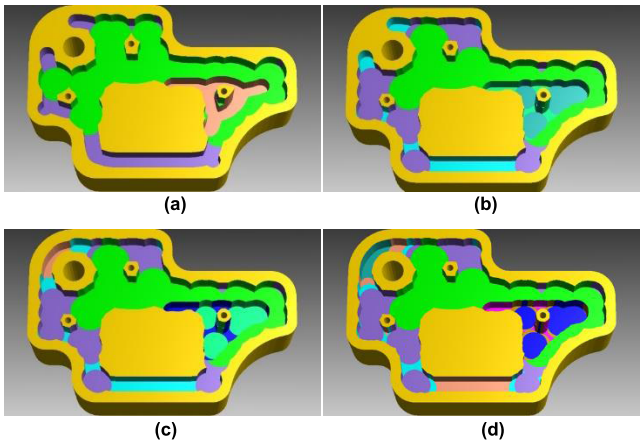


**FIGURE 19. Machining process simulation with different tool groups. (a) 25 and 12. (b) 28, 20, 12. (c) 28, 20, 12, 8. (d) 28, 20, 16, 12, 10.**

left for the finish milling. Therefore, more types of tools can be selected. If the allowed tool types are set to 3, 4 and 5, the corresponding available area ratio can be cut is shown from Table 3 to Table 6, and the simulation results for both layers are shown in Fig. 19. It can be seen that with the increase of allowed tool numbers, the available cut area ratio also increases, but the growth rate is decreasing.

## VII. CONCLUSION

This research proposes an image skeleton based intelligent approach to multiple cutting tools selection for 2 1/2 -axis milling, it can be used for dealing with parts with complex boundaries. The main contribution of this paper can be concluded as follows:

- An accuracy control and rasterization method for converting graphics into images are developed, it built the basis for image-based tool selection.
- A method based on partial differential equations—dynamic skeleton, is used to perform the refinement of the initial skeleton, and accurate image skeleton can be obtained with this method.
- In order to optimize the combination of tool diameters, an objective function based on the residual area of the material was established and solved by GA to obtain the optimal tool combination for a given number of tools.

Therefore, the developed method can be directly integrated into the CAM software for optimal tool diameter selection for 2 1/2 -axis rough machining. Furthermore, optimized toolpath generation based on selected tools as well tool load optimization will be carried out.

## REFERENCES

[1] M. Luo, D. Yan, B. Wu, and D. Zhang, "Barrel cutter design and toolpath planning for high-efficiency machining of freeform surface," *Int. J. Adv. Manuf. Technol.*, vol. 85, no. 9, pp. 2495–2503, 2016.
[2] S. Sui, Y. Li, W. Shao, and P. Feng, "Tool path generation and optimization method for pocket flank milling of aircraft structural parts based on the constraints of cutting force and dynamic characteristics of machine tools," (in English), *Int. J. Adv. Manuf. Technol.*, vol. 85, nos. 5–8, pp. 1553–1564, 2015.
[3] M. Luo, H. Luo, D. Zhang, and K. Tang, "Improving tool life in multi-axis milling of Ni-based superalloy with ball-end cutter based on the active cutting edge shift strategy," *J. Mater. Process. Technol.*, vol. 252, pp. 105–115, Feb. 2018.
[4] Z. Yao, S. K. Gupta, and D. S. Nau, "Algorithms for selecting cutters in multi-part milling problems," *Comput.-Aided Des.*, vol. 35, no. 9, pp. 825–839, 2003.
[5] D. Veeramani and Y.-S. Gau, "Selection of an optimal set of cutting-tool sizes for 2D pocket machining," *Comput.-Aided Des.*, vol. 29, no. 12, pp. 869–877, 1997.
[6] T. Lim, J. Corney, and D. E. R. Clark, "Exact tool sizing for feature accessibility," *Int. J. Adv. Manuf. Technol.*, vol. 16, no. 11, pp. 791–802, 2000.
[7] T. Lim, J. Corney, J. M. Ritchie, and D. E. R. Clark, "Optimizing tool selection," *Int. J. Prod. Res.*, vol. 39, no. 6, pp. 1239–1256, 2001.
[8] Y.-S. Lee and T.-C. Chang, "Application of computational geometry in optimizing 2.5D and 3D NC surface machining," *Comput. Ind.*, vol. 26, no. 1, pp. 41–59, 1995.
[9] Z. C. Chen and H. Zhang, "Optimal cutter size determination for 21/2-axis finish machining of NURBS profile parts," *Int. J. Prod. Res.*, vol. 47, no. 22, pp. 6279–6293, 2009.
[10] Z. C. Chen and Q. Fu, "An optimal approach to multiple tool selection and their numerical control path generation for aggressive rough machining of pockets with free-form boundaries," *Comput.-Aided Des.*, vol. 43, no. 6, pp. 651–663, 2011.
[11] S.-H. Kim and Y. Woo, "Determination of maximum cutter sizes for planar milling by virtual corner detection," (in English), *Int. J. Precis. Eng. Manuf.*, vol. 14, no. 9, pp. 1565–1570, 2013.
[12] M. Mejia-Ugalde, M. Trejo-Hernandez, A. Dominguez-Gonzalez, R. A. Osornio-Rios, and J. P. Benitez-Rangel, "Directional morphological approaches from image processing applied to automatic tool selection in computer numerical control milling machine," *Proc. Inst. Mech. Eng., B, J. Eng. Manuf.*, vol. 227, no. 11, pp. 1607–1619, 2013.
[13] Z. C. Chen and G. Liu, "An intelligent approach to multiple cutters of maximum sizes for three-axis milling of sculptured surface parts," *J. Manuf. Sci. Eng.*, vol. 131, no. 1, p. 014501, 2008.
[14] Z. Ahmad, K. Rahmani, and R. M. D'Souza, "Applications of genetic algorithms in process planning: Tool sequence selection for 2.5-axis pocket machining," (in English), *J. Intell. Manuf.*, vol. 21, no. 4, pp. 461–470, 2010.

[15] V. Sintunata and T. Aoki, "Skeleton extraction in cluttered image based on delaunay triangulation," in *Proc. IEEE Int. Symp. Multimedia (ISM)*, Dec. 2016, pp. 365–366.
[16] J. Wu, H. Duan, and Q. Zhong, "3D image skeleton algorithms," in *Proc. IEEE Int. Conf. Anti-Counterfeiting, Secur. Identificat.*, Jun. 2011, pp. 97–100.
[17] H. Sundar, D. Silver, N. Gagvani, and S. Dickinson, "Skeleton based shape matching and retrieval," in *Proc. Shape Modeling Int.*, May 2003, pp. 130–139.
[18] J. Matute, A. C. Telea, and L. Linsen, "Skeleton-based scagnostics," *IEEE Trans. Vis. Comput. Graphics*, vol. 24, no. 1, pp. 542–552, Jan. 2018.
[19] B.-K. Jang and R. T. Chin, "Analysis of thinning algorithms using mathematical morphology," *IEEE Trans. Pattern Anal. Mach. Intell.*, vol. 12, no. 6, pp. 541–551, Jun. 1990.
[20] C. W. Niblack, P. B. Gibbons, and D. W. Capson, "Generating skeletons and centerlines from the distance transform," *CVGIP, Graph. Models Image Process.*, vol. 54, no. 5, pp. 420–437, 1992.
[21] J. W. Brandt and V. R. Algazi, "Continuous skeleton computation by Voronoi diagram," *CVGIP, Image Understand.*, vol. 55, no. 3, pp. 329–338, 1992.
[22] B. B. Kimia, A. Tannenbaum, and S. W. Zucker, "Shapes, shocks, and deformations I: The components of two-dimensional shape and the reaction-diffusion space," (in English), *Int. J. Comput. Vis.*, vol. 15, no. 3, pp. 189–224, 1995.
[23] M. Kass, A. Witkin, and D. Terzopoulos, "Snakes: Active contour models," *Int. J. Comput. Vis.*, vol. 1, no. 4, pp. 321–331, 1988.

**JING WANG** was born in Xi'an, China, in 1986. He received the B.S. degree in aircraft manufacturing engineering and the M.S. degree in aeronautical and astronautical manufacturing engineering from Northwestern Polytechnical University, Xi'an, in 2009 and 2014, respectively, where he is currently pursuing the Ph.D. degree. His main research interest is multi-axis machining.

**MING LUO** (M'15) received the B.S., M.S., and Ph.D. degrees in aeronautical and astronautical manufacturing engineering from Northwestern Polytechnical University, Xi'an, China, in 2005, 2008, and 2012, respectively. He was a Visiting Scholar with the University of Nottingham in 2016.

From 2012 to 2017, he was an Assistant Research Fellow with the Key Laboratory of Contemporary Design and Integrated Manufacturing Technology, Ministry of Education, Northwestern Polytechnical University. Since 2017, he has been an Associate Research Fellow with the Key Laboratory of Contemporary Design and Integrated Manufacturing Technology. He has authored over 50 articles. He holds four patents. His research interest includes multi-axis machining, data-driven intelligent machining, machining process monitoring, and optimization. He is an Invited Reviewer for many international journals, such as the IEEE/ASME Transactions on Mechatronics, the *International Journal of Machine Tools and Manufacture*, the *Computer-Aided Design*, the *Mechanical Systems and Signal Processing*, and the *Journal of Materials Processing Technology*. He was a Guest Editor of the *International Journal of Manufacturing Research*.

**HAFIZ M. HAFEEZ** received the B.S. degree in mechanical engineering from Northwestern Polytechnical University, Xi'an, China, in 2015. He was a Research Assistant with the Key Laboratory of Contemporary Design and Integrated Manufacturing technology, Northwestern Polytechnical University, in 2015. He is currently a Technical Support Engineer with the Beijing Jingdiao Group Co., Ltd., which is a high-tech corporation and manufacturing CNC engraving centers. He is a member of the American Society of Mechanical Engineers and the Institution of Mechanical Engineers.

**DINGHUA ZHANG** was born in Chengdu, China, in 1958. He received the B.S., M.S., and Ph.D. degrees in advanced manufacturing engineering from Northwestern Polytechnical University, Xi'an, China, in 1981, 1984, and 1989, respectively.

He was with Cornell University, Ithaca, NY, USA, and Rochester University, Rochester, NY, USA, as a Visiting Scholar, from 1996 to 1999. He is currently the Director of the Key Laboratory of Contemporary Design and Integrated Manufacturing Technology, Ministry of Education, Northwestern Polytechnical University. His research interests include smart NC machining, mold design and manufacturing, digital manufacturing system, and digital testing. He is a member of the American Society of Mechanical Engineers, the Chinese Mechanical Engineering Society, and the Chinese Aerospace Society.

Dr. ZHANG has received the First Prize of Shaanxi Scientific and Technological Progress for the NPU—an Interactive Computer Graphics NC programming System in 1991, the Third Prize of National Scientific and Technological Progress for the Development and Application of a CAD/CAM System for Turbo-machinery in 1992, the First Prize of Scientific and Technological Progress (Aero-Industrial Ministry, China) for the Precision Casting Mold CAD/CAM system for Hollow Turbine-Blade of Aero-engine in 1999, and the SPIE Medical Imaging'99 Honorable mention Award for the Accurate and Efficient Calibration Method for a Selenium Flat-panel Detector-based Volume Tomographic Angiography Imaging System, and the Second Prize of National Scientific and Technological Progress for the Development and Application of Precision Five-Axis NC Machining Technology for Turbine Blisk of Aero-Engine in 2006.